Communication

Polyoxometalate-Cyclodextrin Metal-Organic Frameworks: From Tunable Intrinsic Microporosity to Customized Storage Functionality

Peng Yang, Wenli zhao, Aleksander Shkurenko, Youssef Belmabkhout, Mohamed Eddaoudi, Xiaochen Dong, Husam N. Alshareef, and Niveen M Khashab

J. Am. Chem. Soc., **Just Accepted Manuscript** • DOI: 10.1021/jacs.8b11998 • Publication Date (Web): 04 Jan 2019

Polyoxometalate−Cyclodextrin Metal−Organic Frameworks: From Tunable Structure to Customized Storage Functionality

Peng Yang, † Wenli Zhao, ‡ Aleksander Shkurenko, § Youssef Belmabkhout, § Mohamed Eddaoudi, § Xiaochen Dong, ‡ Husam N. Alshareef, ▽ and Niveen M. Khashab †,*

† Smart Hybrid Materials Research Group (SHMs), Advanced Membranes and Porous Materials Center (AMPMC), King Abdullah University of Science and Technology (KAUST), Thuwal 23955, Saudi Arabia.

‡ School of Physical and Mathematical Sciences, Nanjing Tech University, Nanjing 211800, China.

§ Functional Materials Design, Discovery and Development Research Group (FMD3), Advanced Membranes and Porous Materials Center (AMPMC), King Abdullah University of Science and Technology (KAUST), Thuwal 23955, Saudi Arabia.

▽ Materials Sciences and Engineering, Physical Science and Engineering Division, King Abdullah University of Science and Technology (KAUST), Thuwal 23955, Saudi Arabia.

Supporting Information Placeholder

ABSTRACT: Self-assembly allows structures to organize themselves into regular patterns by using local forces to find the lowest-energy configuration. However, assembling organic and inorganic building blocks in an ordered framework is hampered by the difficulties of interfacing two dissimilar materials. Herein, the ensemble of polyoxometalates (POMs) and cyclodextrins (CDs) as molecular building blocks (MBBs) has yielded two unprecedented POM-CD-MOFs, namely $[PW_{12}O_{40}]^{3-}$ & α-CD MOF (**POT-CD**) and $[P_{10}P_{15.5}O_{50}]^{19-}$ & γ-CD MOF (**POP-CD**), with distinct properties not shared by their isolated parent MBBs. Markedly, the **POT-CD** features a nontraditional enhanced Li storage behavior by virtue of a unique "amorphization & pulverization" process. This opens the door to a new generation of hybrid materials with tuned structures and customized functionalities.

With superior properties like chemical tunability and controlled functionalities,[1] metal–organic frameworks (MOFs) figure prominently in significant applications, most notably gas storage,[2] catalysis,[3] sensing,[4] chemical separation,[5] and protein delivery.[6] One of the unique features of MOFs is the modularity of their design and synthesis employing molecular building blocks (MBBs), with their points of extension dictating the geometry and conductivity of the resultant MBBs, to guide their self-assembly.[7] Serving as symmetrical and functional modules suited for polymerization, a plethora of MBBs have been used to enrich the repertoire of MOF chemsitry.[8]

Aside from the conventional metal carboxylate clusters, organic macrocycles especially cyclodextrins (CDs) have been drawn into the construction of MOFs as MBBs.[9] This emerging family of CD-MOFs have proved to be a "green" candidate for various high-end uses, including petrochemicals refining and drug delivery.[10] On the other hand, inorganic hosts,[11] such as polyoxometalates (POMs), have been utilized to build POM-organic frameworks (POMOFs) covering a spectacular structural and compositional variety, and a myriad of applications in fundamental and applied sciences.[12]

Identifying discrete organic and inorganic MBBs that spontaneously self-organize into extended frameworks is key for the successful practice of reticular chemistry. Recent advances in the assembly of POMs and CDs has resulted in supramolecular complexes or oligomers without forming multidimensional networks.[13] In an effort to integrate the advantages of both parent species namely, CD-MOFs and POMOFs in one system, a successful preparation of two POM-CD-MOFs is herein reported for the first time. The structural configuration could be manipulated simply via proper selection of POMs bearing different shapes, sizes, and compositions, such as the classical polyoxotungstate (POT), $[PW_{12}O_{40}]^{3-}$ (PW_{12}), and the newly-discovered polyoxopalladate (POP),[14] $[P_{10}P_{15.5}O_{50}]^{19-}$ ($P_{10}Pd_{15.5}$). Construction of such hybrid assemblies with well-defined suprastructures prospects a highly customized platform with superior properties not shared by their independent components, MBBs. Interestingly, the unique combination of the intrinsically porous α-CD with the redox-active PW_{12} yielded a multilayered assembly that may function as anode material in lithium ion battery (LIB) with an exceptional Li storage behavior.

Co-crystallization of the *in situ* formed Keggin-type PW_{12} with α-CD in KCH_3COO/CH_3COOH buffer has resulted in a three-dimensional (3D) framework, $K_{2.5}Na_{2.5}[(PW_{12}O_{40})(CH_3COO\subset\alpha\text{-CD})(OH)]\cdot 19H_2O$ (**POT-CD**), as characterized and formulated by X-ray structural analysis. The asymmetric unit is composed of one crystallographically independent α-CD and PW_{12} bridged by K^+ and Na^+ cations, of which the coordination spheres are completed by oxygen atoms mainly from the hydroxy groups of α-CD and terminal oxygens of PW_{12}, as well as water molecules (Figure S1). Such a

connection leads to sub-layer A and B that hold the same structural pattern (Figure S2). Their staggered overlap yields a double layer with a certain offset distance, which serves as the basic repeating unit and extends along the *c* axis to give rise to a 3D framework via sharing the metal sites in between (Figures 1a and S3). With deeper insight into the double-layer entity, the α-CD toroids nestled in neighboring sub-layers adopt opposite directions, whereas the PW_{12} moieties rotated horizontally by 90° (Figure 1b). As a consequence of the synthetic media, one acetate anion is encapsulated by an α-CD to fulfill a host–guest assembly, as corroborated by both X-ray diffraction and NMR techniques (Figures S1 and S4).

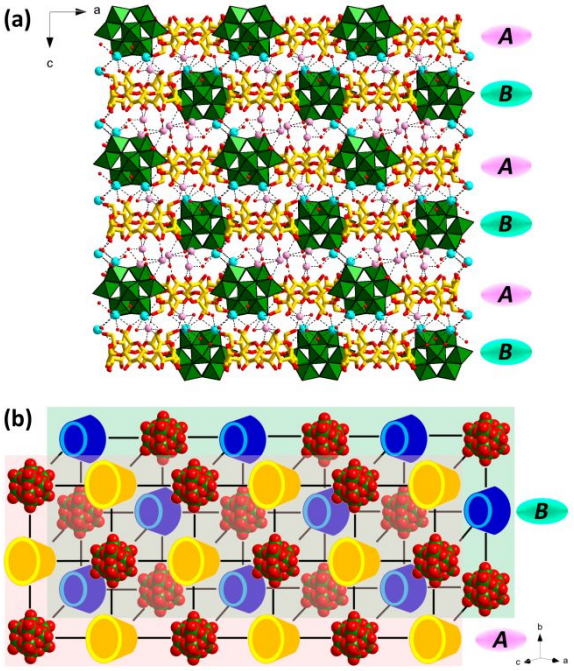

Figure 1. (a) Combined polyhedral/ball-and-stick representation of **POT-CD**. Color code: WO_6, green octahedra; PO_4, pink tetrahedra; K, turquoise; Na, magenta; O, red; C, yellow. (b) A schematic representation of the double-layer repeating unit.

Prompted by the above findings, we intentionally replaced the POM MBBs from the T_d symmetric PW_{12} with a $P_{10}Pd_{15.5}$ having a pseudo-D_{5h} symmetry.[15] As expected, by the help of K^+ linkage, the combination of the star-shaped $P_{10}Pd_{15.5}$ with γ-CD led to a distinct 3D framework, $K_{23}H_{15}[(P_{10}Pd_{15.5}O_{50})_2(\gamma\text{-CD})_2]\cdot 120H_2O$ (**POP-CD**). The asymmetric unit consists of two independent γ-CDs and $P_{10}Pd_{15.5}$, whose oxygen functions are mostly coordinated by K^+ ions (Figure S5). Similar to **POT-CD**, the skeleton of **POP-CD** could be disassembled into two sheets as well. By contrast, each sub-layer in the latter is comprised solely of POPs or CDs, respectively, rather than the mixed of both in the former case (Figure S6). Of prime interest, the γ-CDs in **POP-CD** parallelly stack with each other to pillar the framework, forming open channels running along the *a* axis (Figures 2a and S7). Of these, four kinds of γ-CD toroids according to their different orientations could be grouped as a repeating unit in every CD sheet. Such well-ordered motifs interweave with the adjacent POP layers and direct inversely as compared with their counterparts in the alternate CD sheets (Figure 2b). The total potential solvent accessible void volume of **POT-CD** and **POP-CD** was calculated to be 352.7 and 7030.5 Å^3 (7.3% and 21.4% of the respective unit cell volume) using PLATON.[16] Unfortunately, due to the instability under high vacuum upon solvent removal, the BET surface area of the as-made MOFs could not be accessed. However, supported by CO_2 adsorption data, we could partially access the porosity of **POT-CD**, hence confirming its porous feature (Figure S8).

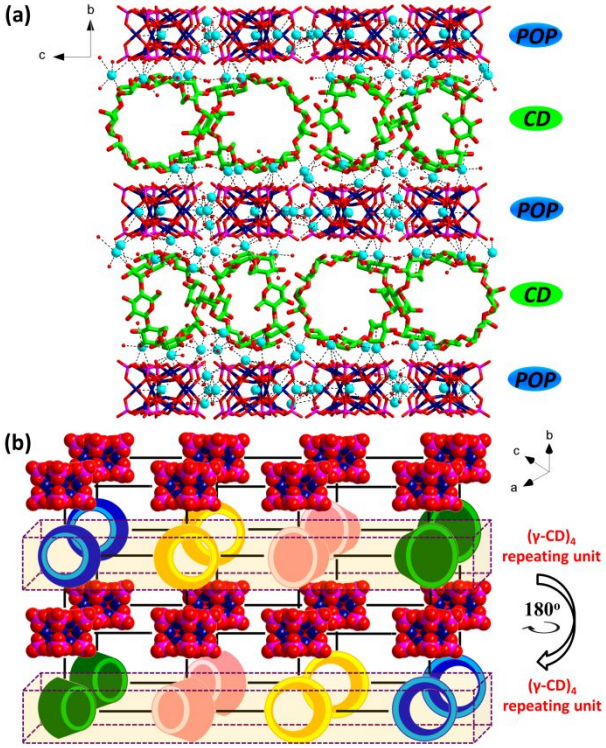

Figure 2. (a) Ball-and-stick representation of **POP-CD**. Color code: Pd, blue; P, pink; K, turquoise; O, red; C, green. (b) A schematic representation of the $(\gamma\text{-CD})_4$ repeating unit.

In light of the above-mentioned, it is believed that, the structural modulation of POM-CD-MOFs is accessible simply via pairing of diverse CD and POM MBBs. More importantly, within the rich arsenal of POMs, such hybrid assemblies can be designed with customized functionalities. In this work, by means of the reversible multielectron redox behavior and electron storage functions of POTs, the electrochemical performance of **POT-CD** as anode material in LIB was evaluated. The charge/discharge voltage profiles of the **POT-CD** anode for different cycles are displayed in Figure 3a. The first discharge and charge capacities of 532 mAh/g and 132 mAh/g are obtained, respectively, with an initial coulombic efficiency (CE) of 25 %. The irreversible capacity loss results principally from the formation of a solid electrolyte interphase (SEI) film due to electrolyte decomposition. The cyclic voltammetry (CV) curves exhibit a broad cathodic peak at about 0.5 V in the first cycle, which could be associated with the SEI formation (Figure S9).[17] In the subsequent cycles, two indistinct peaks became visible at a potential of 0.9 V and 1.1 V, signifying an electrochemical process involving the reduction and oxidation of W in PW_{12}. Meanwhile, the redox reaction of W pre/post cycling was verified unambiguously using XPS results (Figure S10). To further assess the battery performance, cycling stability test was carried out. As illustrated in Figure 3b, after the first few cycles, the CE of **POT-CD** quickly reached a plateau at ≈ 99%.

Surprisingly, in stark contrast to typical POMOF anode materials[18], whose capacities gradually degrade, the cycling capacity of **POT-CD** dramatically rose up as a function of cycle numbers. Detailed inspection shows that a sharp increase in capacity (up to 577 mAh/g) occurs during the first *ca.* 150 cycles, which is substantially higher than that of the first cycle. The cycling capacity steadily reached 695 mAh/g at the 450th cycle, and basically stabilized at this value for another 20 runs afterwards (Figure S11). Notably, the capacity retention achieved an astonishing 482.6% by comparing the capacity of the 450th with the 2nd cycle, indicating an unusual enhanced Li storage behavior.

To unveil this nontraditional phenomenon, a combination of PXRD and SEM characterizations has been utilized to monitor the **POT-CD** anode material before and after the cycling process. Despite the high stability of **POT-CD** in the electrolyte (Figure S12), its PXRD pattern displayed no sharp peaks after the 1st discharge-charge cycle, indicating an amorphous state (**a-POT-CD**, Figure S13). At the same time, a stepwise pulverization process of the MOF-derived **a-POT-CD** has been observed by SEM. Before the cycling test, the crystals of **POT-CD** after grinding (diameter of *ca.* 10-15 μm) have been uniformly distributed on the surface of the anode (Figure S14). Within the first 150 cycles, the size of the **a-POT-CD** decreased dramatically from the order of micron to nanosized particles with diameter of *ca.* 250 nm (Figure S15a-e). Such a powdery degradation gradually slowed down, and the morphology of the nanoparticles remained nearly constant over 150th cycles (Figure S15f). Based on the above, the upswing of cycling capacity could be assigned to a unique "amorphization & pulverization" process: i) because of the relatively weak linkages (e.g., K/Na···O bonds) between MBBs in **POT-CD**, the high lithiation process may proceed through Li coordination by occupying the rich binding sites donated by CDs (hydroxy groups) and POTs (surface oxygens). The bond cleavage of the original framework would lead to the collapse of the skeleton and transformation to the **a-POT-CD**, of which the amorphous state is capable of providing more cation/anion vacancies, void spaces, cluster gaps or interstitial sites for Li storage.[19] ii) due to the electrochemical milling effect,[20] the active material (**a-POT-CD**) could become smaller (pulverization) along with cycle numbers. Consequently, more surface-active sites would be exposed for Li intercalation/ deintercalation. The change of morphology is in good agreement with the obtained cycling capacity, which significantly increased (2nd to 150th cycles) accompanied by a drastic pulverization, and slowly reached a steady state as the size of the nanoparticles remained stable. Furthermore, as a control experiment, the insoluble $(NBu_4)_3[PW_{12}O_{40}]$, α-CD, and their manually mixed analogue (PW_{12} : α-CD = 1 : 1) have been prepared as referenced anodes, of which the capacities achieved only 35 mAh/g (100 mA/g), 45 mAh/g (100 mA/g), and 40 mAh/g (200 mA/g), respectively (Figures S16-S18). It could be concluded that **POT-CD** is indispensable for the "amorphization & pulverization" process and the exceptional Li storage function. Additionally, an electrochemical study of the **POP-CD** anode revealed a limited capacity of 85 mAh/g (100 mA/g), which could be ascribed to the irreversible reduction of POPs into the Pd^0 film (Figures S19).[15a]

The cycling and rate performance of the **POT-CD** anode (after cycling test) were examined. Reversible capacities of 688 mAh/g (at 100 mA/g) and 360 mAh/g (at 1 A/g) were obtained (Figure 4a). When the current density was switched back to 100 mA/g after 25 cycles, the capacities were perfectly restored to the original state, suggesting a good reversibility of the **POT-CD** electrode. Moreover, electrochemical impedance spectroscopy (EIS) was conducted to determine the internal resistance of the test battery. Both Nyquist plots of **POT-CD** show a typical semicircle derived from the charge transfer impedance through the electrode/electrolyte interface (Figure 4b). The charge transfer resistance drops drastically from *ca.* 280 Ω in the first cycle to 38 Ω after 300 discharge-charge cycles, which suggests an improvement of the conductive framework in the anode during discharge-charge process and act in concert with the cycling capacity results.

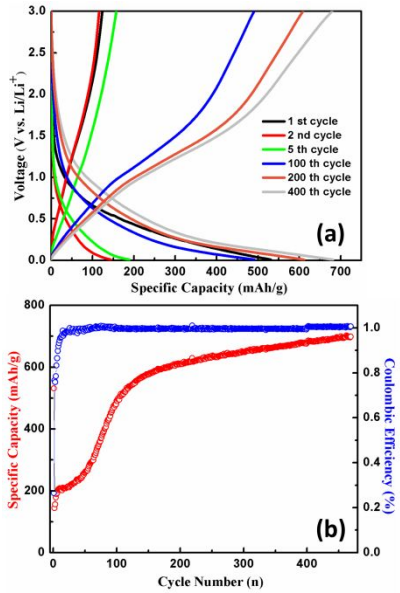

Figure 3. The **POT-CD** anode: (a) Charge-discharge curves for different cycles at 100 mA/g. (b) Cycling performance and coulombic efficiencies at 100 mA/g.

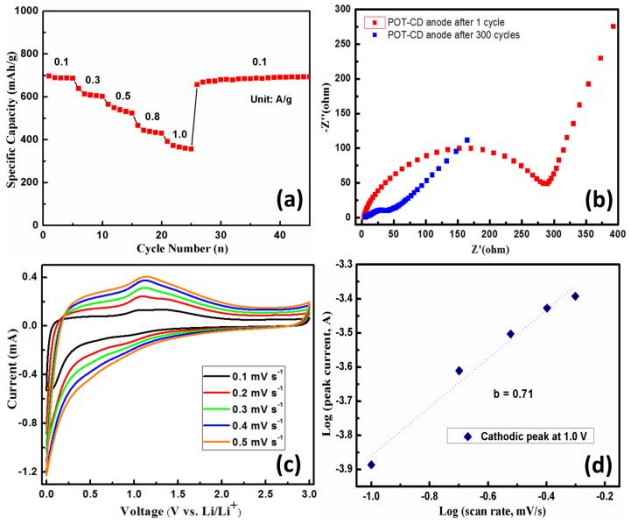

Figure 4. (a) Rate performance at current densities from 100 mA/g to 1 A/g. (b) Nyquist plots at the open circuit potential after the 1st and 300th discharge-charge process. (c) CV profiles recorded at various scan rates from 0.1 to 0.5 mV s^{-1}. (d) The logarithmic relationship between currents and scan rates for the **POT-CD** anode.

To further understand the charge storage mechanisms of

the **POT-CD** electrode, CVs were measured at different scan rate between 0.01–3.0 V (Figure 4c). According to the power law $i = a \times v^b$,[21] a good linear relationship is observed between log(*i*) and log(*v*). Herein, a *b*-value of 0.71 was measured for **POT-CD**, signifying the charge storage arises from both diffusion and capacitive processes (Figure 4d): Li^+ insertion/extraction (diffusion controlled behavior in the bulk phase) and pseudocapacitive mechanism (ion transfer behavior on the surface and/or near surface area). In this case, the MOF-derived **a-POT-CD** with amorphous structure and increased surface area is beneficial to the facile lithiation/delithiation kinetics through a short-length diffusion process and an intercalation pseudocapacitance occurs on the surface of the anode material.[22]

In conclusion, the first two examples of POM-CD-MOFs have been prepared via a facile solution technique and well characterized by a multitude of physicochemical techniques. The results showcase that both POMs and CDs could assume the role of MBBs to effectively program the structure with functional enrichment. As a proof of concept, an interesting upswing of cycling capacity in the **POT-CD** anode material might be assigned to a unique "amorphization & pulverization" process for improving the Li ion storage. It can be foreseen that functional oriented complexation of multifarious POMs and CDs will open intriguing prospects for aiding the transition from discovery to design of POM-CD-MOFs with "built-in" functionalization for state of the art applications.

ASSOCIATED CONTENT

Supporting Information

The Supporting Information is available free of charge on the ACS Publications website at DOI...

Experimental details, and supporting figures and tables (PDF) Crystallographic data (CIF)

AUTHOR INFORMATION

Corresponding Author

*niveen.khashab@kaust.edu.sa

Author Contributions

P.Y. and W.Z. contributed equally.

Notes

The authors declare no competing financial interest.

ACKNOWLEDGMENTS

Authors acknowledge Dr. G. Mouchaham and Dr. O. El-Tall for technical assistance.

REFERENCES

(1) Furukawa, H.; Cordova, K. E.; O'Keeffe, M.; Yaghi, O. M. The chemistry and applications of metal–organic frameworks. *Science* **2013**, *341*, 1230444.

(2) Islamoglu, T.; Goswami, S.; Li, Z.; Howarth, A. J.; Farha, O. K.; Hupp, J. T. Postsynthetic Tuning of Metal–Organic Frameworks for Targeted Applications. *Acc. Chem. Res.* **2017**, *50*, 805–813.

(3) Jiao, L.; Wang, Y.; Jiang, H.-L.; Xu, Q. Metal–Organic Frameworks as Platforms for Catalytic Applications. *Adv. Mater.* **2018**, *30*, 1703663.

(4) Lu, K.; Aung, T.; Guo, N.; Weichselbaum, R.; Lin, W. Nanoscale Metal–Organic Frameworks for Therapeutic, Imaging, and Sensing Applications. *Adv. Mater.* **2018**, *30*, 1707634.

(5) Li, B.; Wen, H.-M.; Cui, Y.; Zhou, W.; Qian, G.; Chen, B. Emerging Multifunctional Metal–Organic Framework Materials. *Adv. Mater.* **2016**, *28*, 8819–8860.

(6) Alsaiari, S. K.; Patil, S.; Alyami, M.; Alamoudi, K. O.; Aleisa, F. A.; Merzaban, J. S.; Li, M.; Khashab, N. M. Endosomal Escape and Delivery of CRISPR/Cas9 Genome Editing Machinery Enabled by Nanoscale Zeolitic Imidazolate Framework. *J. Am. Chem. Soc.* **2018**, *140*, 143–146.

(7) Eddaoudi, M.; Moler, D. B.; Li, H.; Chen, B.; Reineke, T. M.; O'Keeffe, M.; Yaghi, O. M. Modular Chemistry: Secondary Building Units as a Basis for the Design of Highly Porous and Robust Metal–Organic Carboxylate Frameworks. *Acc. Chem. Res.* **2001**, *34*, 319–330.

(8) Tranchemontagne, D. J.; Mendoza-Cortés, J. L.; O'Keeffe, M.; Yaghi, O. M. Secondary building units, nets and bonding in the chemistry of metal–organic frameworks. *Chem. Soc. Rev.* **2009**, *38*, 1257–1283.

(9) Smaldone, R. A.; Forgan, R. S.; Furukawa, H.; Gassensmith, J. J.; Slawin, A. M. Z.; Yaghi, O. M.; Stoddart, J. F. Metal–Organic Frameworks from Edible Natural Products. *Angew. Chem., Int. Ed.* **2010**, *49*, 8630–8634.

(10) (a) Gassensmith, J. J.; Furukawa, H.; Smaldone, R. A.; Forgan, R. S.; Botros, Y. Y.; Yaghi, O. M.; Stoddart, J. F. Strong and Reversible Binding of Carbon Dioxide in a Green Metal–Organic Framework. *J. Am. Chem. Soc.* **2011**, *133*, 15312–15315. (b) Wu, D.; Gassensmith, J. J.; Gouvêa, D.; Ushakov, S.; Stoddart, J. F. Navrotsky, A. Direct Calorimetric Measurement of Enthalpy of Adsorption of Carbon Dioxide on CD-MOF-2, a Green Metal–Organic Framework. *J. Am. Chem. Soc.* **2013**, *135*, 6790–6793. (c) Hartlieb, K. J.; Holcroft, J. M.; Moghadam, P. Z.; Vermeulen, N. A.; Algaradah, M. M.; Nassar, M. S.; Botros, Y. Y.; Snurr, R. Q.; Stoddart, J. F. CD-MOF: A Versatile Separation Medium. *J. Am. Chem. Soc.* **2016**, *138*, 2292–2301. (d) Liu, B.; He, Y.; Han, L.; Singh, V.; Xu, X.; Guo, T.; Meng, F.; Xu, X.; York, P.; Liu, Z.; Zhang, J. Microwave-Assisted Rapid Synthesis of γ-Cyclodextrin Metal–Organic Frameworks for Size Control and Efficient Drug Loading. *Cryst. Growth Des.* **2017**, *17*, 1654–1660.

(11) Yang, P.; Alsufyani, M.; Emwas, A.-H.; Chen, C.; Khashab, N. M. Lewis Acid Guests in a $\{P_8W_{48}\}$ Archetypal Polyoxotungstate Host: Enhanced Proton Conductivity via Metal-Oxo Cluster within Cluster Assemblies. *Angew. Chem., Int. Ed.* **2018**, 57, 13046–13051.

(12) (a) Streb, C.; Ritchie, C.; Long, D.-L.; Kögerler, P.; Cronin, L. Modular Assembly of a Functional Polyoxometalate-Based Open Framework Constructed from Unsupported Ag^I...Ag^I Interactions. *Angew. Chem., Int. Ed.* **2007**, *46*, 7579–7582. (b) Du, D.-Y.; Qin, J.-S.; Li, S.-L.; Su, Z.-M.; Lan, Y.-Q. Recent advances in porous polyoxometalate-based metal–organic framework materials. *Chem. Soc. Rev.* **2014**, *43*, 4615–4632.

(13) (a) Izzet, G.; Ménand, M.; Matt, B.; Renaudineau, S.; Chamoreau, L.-M.; Sollogoub, M.; Proust, A. Cyclodextrin-Induced Auto-Healing of Hybrid Polyoxometalates. *Angew. Chem., Int. Ed.* **2012**, *51*, 487–490. (b) Zhang, B.; Yue, L.; Wang, Y.; Yang, Y.; Wu, L. A novel single-side azobenzene-grafted Anderson-type polyoxometalate for recognition-induced chiral migration. *Chem. Commun.* **2014**, *50*, 10823–10826. (c) Wu, Y.; Shi, R.; Wu, Y.-L.; Holcroft, J. M.; Liu, Z.; Frasconi, M.; Wasielewski, M. R.; Li, H.; Stoddart, J. F. Complexation of Polyoxometalates with Cyclodextrins. *J. Am. Chem. Soc.* **2015**, *137*, 4111–4118. (d) Moussawi, M. A.; Leclerc-Laronze, N.; Floquet, S.; Abramov, P. A.; Sokolov, M. N.; Cordier, S.; Ponchel, A.; Monflier, E.; Bricout, H.; Landy, D.; Haouas, M.; Marrot, J.; Cadot, E.

Polyoxometalate, Cationic Cluster, and γ-Cyclodextrin: From Primary Interactions to Supramolecular Hybrid Materials. *J. Am. Chem. Soc.* **2017**, *139*, 12793–12803. (e) Moussawi, M. A.; Haouas, M.; Floquet, S.; Shepard, W. E.; Abramov, P. A.; Sokolov, M. N.; Fedin, V. P.; Cordier, S.; Ponchel, A.; Monflier, E.; Marrot, J.; Cadot, E. Nonconventional Three-Component Hierarchical Host–Guest Assembly Based on Mo-Blue Ring-Shaped Giant Anion, γ-Cyclodextrin, and Dawson-type Polyoxometalate. *J. Am. Chem. Soc.* **2017**, *139*, 14376–14379. (f) Falaise, C.; Moussawi, M. A.; Floquet, S.; Abramov, P. A.; Sokolov, M. N.; Haouas, M.; Cadot, E. Probing Dynamic Library of Metal-Oxo Building Blocks with γ-Cyclodextrin. *J. Am. Chem. Soc.* **2018**, *140*, 11198–11201.

(14) (a) Izarova, N. V.; Pope, M. T.; Kortz, U. Noble Metals in Polyoxometalates. *Angew. Chem., Int. Ed.* **2012**, *51*, 9492–9510. (b) Yang, P.; Kortz, U. Discovery and Evolution of Polyoxopalladates. *Acc. Chem. Res*. **2018**, *51*, 1599–1608.

(15) (a) Izarova, N. V.; Ngo Biboum, R.; Keita, B.; Mifsud, M.; Arends, I. W. C. E.; Jameson, G. B.; Kortz, U. Self-assembly of star-shaped heteropoly-15-palladate(II). *Dalton Trans*. **2009**, *43*, 9385–9387. (b) Xu, F.; Scullion, R. A.; Yan, J.; Miras, H. N.; Busche, C.; Scandurra, A.; Pignataro, B.; Long, D.-L.; Cronin, L. A Supramolecular Heteropolyoxopalladate $\{Pd_{15}\}$ Cluster Host Encapsulating a $\{Pd_2\}$ Dinuclear Guest: $[Pd^{II}_2 \subset \{H_7Pd^{II}_{15}O_{10}(PO_4)_{10}\}]^{9-}$. *J. Am. Chem. Soc.* **2011**, *133*, 4684–4686. (c) Yang, P.; Xiang, Y.; Lin, Z.; Bassil, B. S.; Cao, J.; Fan, L.; Fan, Y.; Li, M.-X.; Jiménez-Lozano, P.; Carbó, J. J.; Poblet, J. M.; Kortz, U. Alkaline earth guests in polyoxopalladate chemistry: from nanocube to nanostar via an open-shell structure. *Angew. Chem., Int. Ed*. **2014**, *53*, 11974–11978. (d) Yang, P.; Xiang, Y.; Lin, Z.; Lang, Z.; Jiménez-Lozano, P.; Carbó, J. J.; Poblet, J. M.; Fan, L.; Hu, C.; Kortz, U. Discrete Silver(I)-Palladium(II)-Oxo Nanoclusters, $\{Ag_4Pd_{13}\}$ and $\{Ag_5Pd_{15}\}$, and the Role of Metal-Metal Bonding Induced by Cation Confinement. *Angew. Chem., Int. Ed*. **2016**, 55, 15766–15770.

(16) Sheldrick, G. M. A short history of *SHELX*. *Acta Crystallogr. A* **2008**, *64*, 112–122.

(17) Fong, R.; Sacken, U.; Dahn, J. R. Studies of Lithium Intercalation into Carbons Using Nonaqueous Electrochemical Cells. *J. Electrochem. Soc*. **1990**, *137*, 2009–2013.

(18) (a) Yue, Y.; Li, Y.; Bi, Z.; Veith, G. M.; Bridges, C. A.; Guo, B.; Chen, J.; Mullins, D. R.; Surwade, S. P.; Mahurin, S. M.; Liu, H.; Paranthaman, M. P.; Dai, S. A POM–organic framework anode for Li-ion battery. *J. Mater. Chem. A* **2015**, *3*, 22989–22995. (b) Zhu, P.-P.; Sheng, N.; Li, M.-T.; Li, J.-S.; Liu, G.-D.; Yang, X.-Y.; Sha, J.-Q.; Zhu, M.-L.; Jiang, J. Fabrication and electrochemical performance of unprecedented POM-based metal–carbene frameworks. *J. Mater. Chem. A* **2017**, *5*, 17920–17925. (c) Li, X.-X.; Shen, F.-C.; Liu, J.; Li, S.-L.; Dong, L.-Z.; Fu, Q.; Su, Z.-M.; Lan, Y.-Q. A highly stable polyoxometalate-based metal–organic framework with an ABW zeolite-like structure. *Chem. Commun*. **2017**, *53*, 10054–10057. (d) Huang, Q.; Wei, T.; Zhang, M.; Dong, L.-Z.; Zhang, A.-M.; Li, S.-L.; Liu, W.-J.; Liu, J.; Lan, Y.-Q. A highly stable polyoxometalate-based metal–organic framework with π–π stacking for enhancing lithium ion battery performance. *J. Mater. Chem. A* **2017**, *5*, 8477–8483.

(19) Chae, O. B.; Kim, J.; Park, I.; Jeong, H.; Ku, J. H.; Ryu, J. H.; Kang, K.; Oh, S. M. Reversible Lithium Storage at Highly Populated Vacant Sites in an Amorphous Vanadium Pentoxide Electrode. *Chem. Mater.* **2014**, *26*, 5874–5881.

(20) (a) Yu, Y.; Shi, Y.; Chen, C.-H.; Wang, C. Facile Electrochemical Synthesis of Single-Crystalline Copper Nanospheres, Pyramids, and Truncated Pyramidal Nanoparticles from Lithia/Cuprous Oxide Composite Thin Films. *J. Phys. Chem. C* **2008**, *112*, 4176–4179. (b) Zhao, K.; Liu, F.; Niu, C.; Xu, W.; Dong, Y.; Zhang, L.; Xie, S.; Yan, M.; Wei, Q.; Zhao, D.; Mai, L. Graphene Oxide Wrapped Amorphous Copper Vanadium Oxide with Enhanced Capacitive Behavior for High-Rate and Long-Life Lithium-Ion Battery Anodes. *Adv. Sci*. **2015**, *2*, 1500154.

(21) (a) Simon, P.; Gogotsi, Y.; Dunn, B. Materials science. Where do batteries end and supercapacitors begin? *Science* **2014**, *343*, 1210–1211. (b) Lukatskaya, M. R.; Dunn, B.; Gogotsi, Y. Multidimensional materials and device architectures for future hybrid energy storage. *Nat. Commun.* **2016**, *7*, 12647.

(22) Brezesinski, T.; Wang, J.; Tolbert, S. H.; Dunn, B. Ordered mesoporous α-MoO_3 with iso-oriented nanocrystalline walls for thin-film pseudocapacitors. *Nat. Mater*. **2010**, *9*, 146–151.

TOC

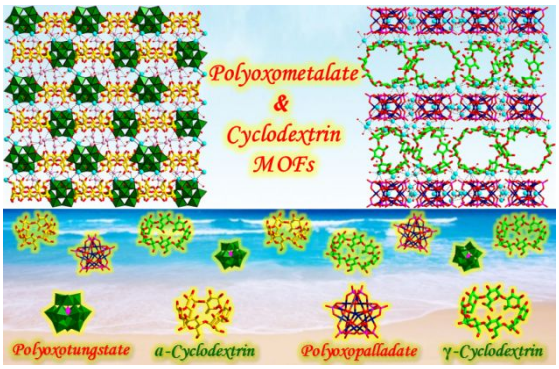
Polyoxometalate
&
Cyclodextrin
MOFs
Polyoxotungstate
a-Cyclodextrin
Polyoxopalladate
γ-Cyclodextrin